JOURNAL OF MATERIALS SCIENCE **39** (2004) 519–528

Morphological features of interfacial intermetallics and interfacial reaction rate in Al-11Si-2.5Cu-(0.15/0.60)Fe cast alloy/die steel couples

G. B. WINKELMAN*
School of Physics and Materials Engineering, Monash University, Australia

Z. W. CHEN*
Faculty of Science and Engineering, Auckland University of Technology, New Zealand

D. H. StJOHN
Cooperative Research Centre for Cast Metals Manufacturing (CAST), University of Queensland, Australia

M. Z. JAHEDI
Cooperative Research Centre for Cast Metals Manufacturing (CAST), CSIRO Manufacturing Science and Technology, Australia

Soldering reactions are commonly observed during high pressure die casting of aluminium alloys, and involve the formation and growth of interfacial intermetallics between the die and the cast alloy. It is generally believed that close to 1% Fe is necessary in the aluminium alloy to reduce soldering. However, the role of iron in the interfacial reaction has not been studied in detail. In this investigation, reaction couples were formed between H13 tool steel substrates and an Al-11Si-2.5Cu melt containing either 0.15 or 0.60% Fe. Examination revealed distinctly different intermetallic layer morphology. The overall growth and chemistry of the reaction layer and the reaction rate measured by the consumption of the substrate were compared for the two alloy melts. It was demonstrated that a higher iron content reduces the rate of interfacial reaction, consistent with an observed thicker compact (solid) intermetallic layer. Hence, the difference in reaction rate can be explained by a significant reduction in the diffusion flux due to a thicker compact layer. Finally, the mechanism of the growth of a thicker compact layer in the higher iron melt is proposed, based on the phase relations and diffusion both within and near the interfacial reaction zone. © *2004 Kluwer Academic Publishers*

1. Introduction

Soldering in high pressure die casting (HPDC) is one of the major causes of die failure and occurs directly as a result of interactions between the die steel and the injected molten aluminium alloy. Soldering is characterised by the formation of intermetallic phases at the interface between the die steel and the molten aluminium alloy [1]. Sticking of the casting alloy to the die, as a direct result of die soldering, can produce defective castings, hinder ejection of the casting from the die and shorten the useful die life [1].

It is generally accepted within the HPDC industry that, to circumvent the soldering reaction, the iron content of a casting alloy must be maintained at or above its saturation point, therefore reducing the chemical potential of Fe dissolution into the melt. This results in the current practice of maintaining approximately 1% Fe in aluminium casting alloys. However, the reduction of iron content in castings is desirable since, as is well known, iron-containing intermetallic particles can adversely affect the mechanical properties of the cast part [2].

Due to its industrial importance, HPDC soldering has been the subject of many studies [1, 3–12]. From these studies, however, very little scientific evidence has been presented to explain the phenomenon of reduced soldering and die steel consumption in the presence of a high iron content. This is reflected by the recent scientific review on the subject by Yan and Fan [13], where very little data on the effect of melt chemistry on reaction rate could be provided. Furthermore, Sundqvist *et al.* based on their immersion experiments using 0.5%

*Formerly with the Cooperative Research Centre for Cast Metals Manufacturing (CAST).

and 1% Fe and weight loss measurement suggested that a high iron content may not necessarily be beneficial for reducing soldering reaction [9]. It is thus the aim of this study to provide scientific evidence to explain the effect of iron content in die cast alloys on the soldering reaction.

Immersion tests are an experimental technique used for the investigation of interfacial interactions between liquids and solids, where a solid sample is immersed into a bath of stationary or agitated liquid. Immersion tests have often been used in investigations addressing the soldering of HPDC dies [3–13], and are employed here in a campaign of experiments targeted at investigating the effect of melt iron content on intermetallic layer morphology and the reaction rate.

The morphological features of the interfacial reaction products are presented, together with a justification of the morphology based on the prevailing compositional conditions. Selected data will also be given to show the effect of iron on the overall growth rate of the intermetallics and concurrent die steel consumption (reaction rate). Based on these observations and data, an explanation for the effect of iron on inhibiting intermetallic growth at the interface is given. Furthermore, based on the theoretical examination of the phase relations and diffusion in the interfacial region, a mechanism is proposed to explain the observed difference in intermetallic layer thickness for different melt iron contents.

2. Experimental procedures

Coupons of 25 mm × 25 mm ×2 mm were fabricated from hot work H13 tool steel and heat treated to a hardness of 42–45 HRC. A chemical analysis of the steel is given in Table I. The base alloy composition (Al-11Si-2.5Cu) was selected with typical HPDC alloys in mind, particularly with regard to the silicon and copper composition. High purity Al and Cu were used as starting materials, while industrial grade silicon, containing a nominal iron content, was used. A chemical analysis of the base aluminium alloy is given in Table II. The iron content in the base aluminium alloy was 0.15% Fe (wt% throughout). Pure electrolytic iron was added to the melt to produce a second alloy containing 0.60% Fe.

TABLE I Chemical analysis of H13 hot-work tool steel

H13 hot work tool steel (wt%)						
Fe	Si	C	Cr	Mo	V	Mn
∼bal	1.05	0.4	5.0	1.35	1.1	0.42

TABLE II Chemical analysis of base aluminium alloy

Aluminium alloy (wt%)			
Al	Si	Cu	Fe
∼bal	10.81	2.50	0.15

The use of 0.60% Fe was based on the consideration of soldering reaction in HPDC. As has been demonstrated [14], under normal HPDC conditions (for aluminium alloys), soldering reaction inside the die cavity takes place at or below the main eutectic temperature. The solubility of Fe in Al-Si eutectic is not certain but is likely to be much lower than 1% [15]. Data from Granger [16] indicates that the solubility of Fe in commercial high pressure die cast alloys may even be lower than 0.7% at the main eutectic point.

For immersion experiments, a silicon carbide crucible was used in an electric furnace and contained approximately 1 kg of the alloy. The melt temperature was controlled using a k-type thermocouple and an auto-setting PID microprocessor-based temperature controller. The thermocouple was placed in a thin-walled ceramic tube to prevent reaction with the melt and the protected thermocouple was positioned near the wall of the crucible. The set point for the melt was 610°C throughout the study.

During immersion of the steel coupon in the aluminium alloy, it was expected that the iron content of the melt would increase due to dissolution of the tool steel substrate. Hence, the iron content of selected melts after immersion experiments was analysed. This was done by removing a small amount of the alloy melt using a small boron-nitride coated ladle, quenching the sample in water, and assaying for iron by the ICP-AES method. Results showed that even for immersion times of up to 1000 s (equal to the longest immersion time used in this study) the extent of this increase is low, resulting in approximate increases of 15 and 4% respectively for the 0.15% Fe and 0.60% Fe alloy melts. Therefore, the potential for misleading results as a consequence of iron enrichment is low.

Upon immersion, there exists an oxide barrier at the interface between the two materials. This oxide barrier prevents intimate contact between the two materials and can vary in thickness from coupon to coupon. Hence, the steel coupons were fluxed prior to immersion in the melt. This involved depositing a solid salt flux onto the surface of the coupon, which, upon immersion into the melt, acted on the oxides present. The fluxing procedure used in this work is based on a sequence described in the literature [17–20] and consists of the following steps, with intermediate rinsing between each step:

- Degreasing in 3% sodium carbonate solution for 5 min. in an ultrasonic bath.
- Anodically degreasing in 3% sodium carbonate solution for 1 min.
- Pickling in 10% hydrochloric acid for 1 min. in an ultrasonic bath.
- Fluxing in a saturated aqueous solution consisting of 30% KCl, 30% NaCl and 10% each of LiCl, KI, KBr and NaF at 70°C for 5 min.

After fluxing, the steel was dried at 70°C for 5 min prior to the immersion experiment. Immersion was carried out for a period of 5 to 1000 s. The melt was not stirred. Immediately following removal from the melt, the coupon was quenched in water (∼20°C) to arrest

the interfacial reaction. Preliminary tests of the two aluminium alloys showed that, at 610°C, there was no intermetallic phase precipitation in the molten alloy, suggesting that the contained iron was fully soluble. This knowledge thus avoided potentially confusing experimental results, and it can therefore be assumed that any intermetallic phases generated during immersion were the result of contact between the steel and the alloy melt, and not pre-immersion artifacts.

After immersion, cross-sectional metallographic samples were prepared following the normal procedures. A Scanning Electron Microscope (SEM) (Leica S440) was used for examination of the interface cross-sections. Compositional analysis of intermetallic phases was carried out using a Link Ge Energy Dispersive Spectroscopy (EDS) detector and Link ISIS software connected to the SEM at 20 kV. The probe current was set at 2.5 nA and a counting time of 100 s was used for each spot analysis. ZAF correction was applied to the accumulated data. It should be noted that the intermetallic layers and the irregularly shaped intermetallic particles chosen for compositional analysis were greater than 3 μm in width.

The thickness and composition of the intermetallic layers formed as a result of the interaction between the steel coupon and the alloy was recorded, as was the thickness of the entire reaction zone existing at the interface. In order to better describe the rate of the consumption of the die steels due to reaction during the immersion, the advance of the steel-intermetallic interface was monitored. By protecting a portion of the surface of the steel coupon from the molten alloy by the application of boron nitride paint, only localized dissolution of the steel coupon was permitted. In cross-section, the depth of steel removed by the reactive aluminium during the interaction period could then be directly measured (Fig. 1).

3. Results

Fig. 2 displays the interface cross-sections of the steel immersed in 0.15% Fe and 0.60% Fe alloy melts for 5 s, 15 s, 65 s and 500 s. It was observed that 5 s immersion in both low and higher iron melts (Fig. 2a and b) allows the formation of angular phases near the interface between the steel coupon and the adhered aluminium alloy. These angular particles were small in number and a very high portion of the interface was free of these particles. Qualitative observation, however, suggests that these angular phases are greater in number and size for the case of immersion in the 0.60% Fe alloy after 5 s immersion.

The angular phases disappear after 15 s immersion in the low iron melt. On the other hand, in the high iron melt, interface examination reveals larger angular particles after 15 s immersion. After 65 s, the plate-like particles at the interface have grown, and exhibit a reduced aspect ratio. Although it is not shown in Fig. 2, overall examination revealed that the particles covered less than 20% of the total interfacial area. Being localized, the presence of these particles at the interface, identified as the β-phase intermetallic $FeSiAl_5$, does not affect the overall interfacial reaction of the remaining reaction area. The microstructural evolution of these particles and the conditions that enable it to form will be addressed in a subsequent communication [21] and will not be discussed further in this paper.

3.1. Morphology and composition of the intermetallic layers

Following 15 s immersion in the *low* iron melt (Fig. 2c), there appears to be a thin reaction layer at the interface. Following 65 s of immersion (Fig. 2e), a clearly defined reaction product in the form of a "compact" intermetallic layer 2 to 3 μm in thickness and in contact with the

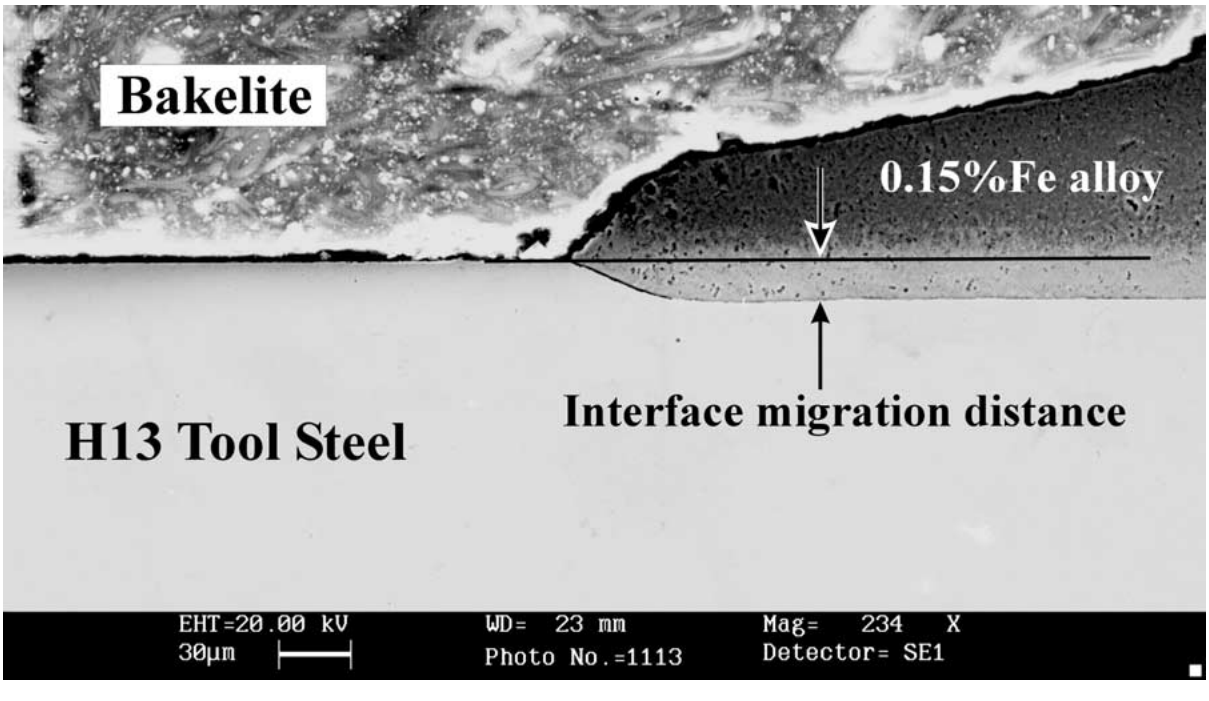

Figure 1 A cross-sectional micrograph showing the distance that the interface migrates during immersion for 500 s in a 0.15% Fe aluminium alloy at 610°C.

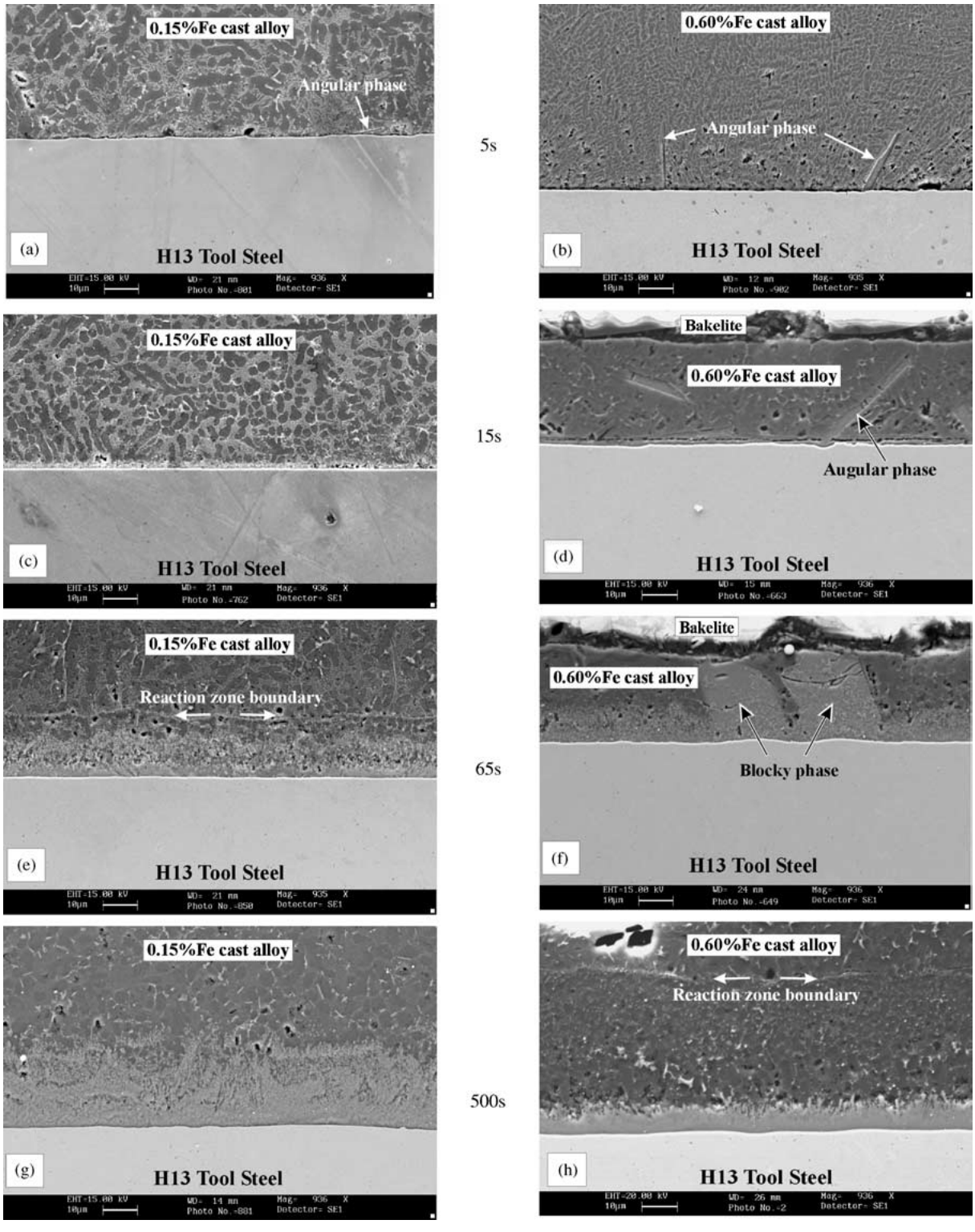

Figure 2 Interface cross-section of H13 tool steel immersed in Al-11Si-2.5Cu-0.15Fe [(a), (c), (e) and (g)] and Al-11Si-2.5Cu-0.60Fe alloy [(b), (d), (f) and (h)] for 5 s, 15 s, 65 s and 500 s respectively.

steel surface is observed. Adjacent to this compact layer is a second layer extending to $\sim$10 μm from the steel substrate, consisting of loosely arranged, but still quite dense intermetallic phases. We denote this layer as the "broken" intermetallic layer.

Adjacent to the broken layer is a yet another distinct layer $\sim$5 μm in thickness, where many individual intermetallic particles can still be seen, evidently suspended in matrix of aluminium alloy. This latter region is termed the "floating" intermetallic layer and is bounded by the Reaction Zone Boundary (RZB) as marked in Fig. 2e. Beyond the RZB, the concentration of intermetallic particles appears to be much reduced, and the aluminium alloy in this region is referred to as the bulk alloy.

After a contact period of 500 s in the low iron melt (Fig. 2g), the reaction zone has become considerably thicker (RZB is not able to be shown in Fig. 2g). Although initially appearing to be characterised by a thick intermetallic layer, close examination (Fig. 3a) reveals

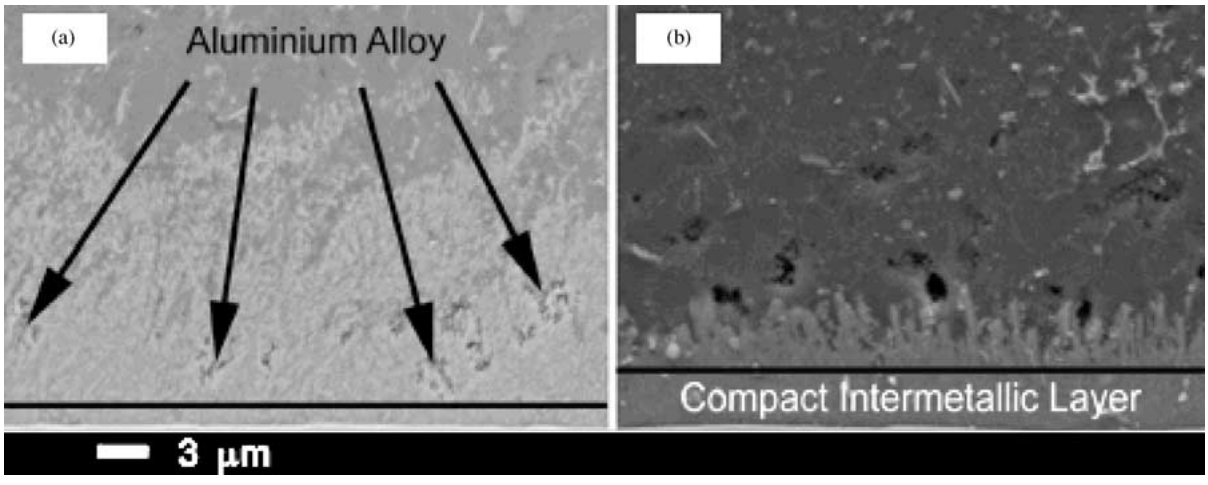

Figure 3 Interface cross-sections of samples immersed for 500 s in (a) 0.15%Fe and (b) 0.60%Fe aluminium alloy melts.

that a large proportion of the reaction product qualifies as a broken intermetallic layer by virtue of its discontinuous nature. Within this layer, the material in the darker regions appears similar in texture and shade to the aluminium alloy outside the layer. It is therefore assumed that the dark regions within the broken layer, as indicated in Fig. 3a, are aluminium alloy which was in liquid state during immersion. The compact intermetallic layer itself is only 2–3 μm in thickness, and hence only represents a small proportion of the reaction product layer.

In contrast to the 0.15% Fe melt, the reaction product layer formed adjacent to the steel substrate during immersion in the 0.60% Fe melt appears to be comprised of a thicker compact layer (Fig. 2f and h). This is better shown in Fig. 3 (immersion time of 500 s), where the compact layers formed in both low and higher iron melts are directly compared. The higher iron melt (Fig. 3b) allows the formation of a uniform and thicker compact intermetallic layer, lying contiguous with the tool steel. The lower iron melt (Fig. 3a) produces a thinner compact intermetallic layer, as previously noted. In similarity to immersion in the low iron melts, a broken intermetallic layer is formed between the compact layer and aluminium alloy within the reaction zone. It is noted that the thickness of the broken intermetallic layer is considerably less than the thickness of the equivalent layer in the lower iron melt.

Two typical EDS analyses of the compact layers grown following 500 s immersion are presented in Fig. 4a and b, for the 0.15% Fe and 0.60% Fe alloys respectively. For both cases, the intermetallic in the compact layer is found to contain major elements of aluminium, iron and silicon and smaller percentages of chromium and copper. These compositions indicate that the compact intermetallic layer is likely to be a phase isomorphous with α_H-Fe_2SiAl_8 containing small amounts of chromium and copper [3].

3.2. Layer thickness measurement

Results of measurements of layer thickness are given in Fig. 5. Fig. 5a shows that, for immersion in the 0.15% Fe melt, the compact layer only marginally increases in thickness while immersed from 65 s to 500 s. It should be noted that, due to the morphological nature of the interfacial layers generated in the 0.15% Fe melt, the measurement of the compact layer is expected to be less certain in comparison to the other layers. The broken layer thickness, however, increases significantly, as does the distance separating the RZB and the H13/compact layer interface.

In contrast, measurements have shown that the compact layer significantly increases in thickness as immersion time increases during immersion in the high iron melt. It should be noted that thickness measurements of the compact layer in the higher iron samples is significantly more certain due to the layer being more distinctive in appearance. The broken layer, however, actually reduces in thickness as the immersion time is increased. It is therefore clear that, while there is a considerably thicker *total* (compact + broken) intermetallic layer in the case of immersion in the 0.15% Fe alloy, immersion in the higher iron alloy results in a thicker compact intermetallic layer.

Measurements of actual H13 tool steel consumption (or the interface migration distance, IMD) are plotted in Fig. 6. It should be noted that for this measurement of interface migration, the measurement itself becomes increasingly uncertain for immersion times less then 300 s, since the IMD is very small. Hence, data could only be provided for the cases where immersion times are 300 s and higher. It can be observed from Fig. 6 that the IMD is considerably smaller, particularly for long immersion times, in the case of immersion in the higher iron melt.

4. Discussion

Despite the apparent differences in morphology of the interfacial intermetallics formed in the low iron melt compared to the high iron melt, the interfacial reaction zone can be discussed with reference to a schematic illustration, as provided in Fig. 7. This figure depicts the interface for the general case at time "*t*", characterised by the compact intermetallic layer (solid), the broken intermetallic layer and the floating intermetallic

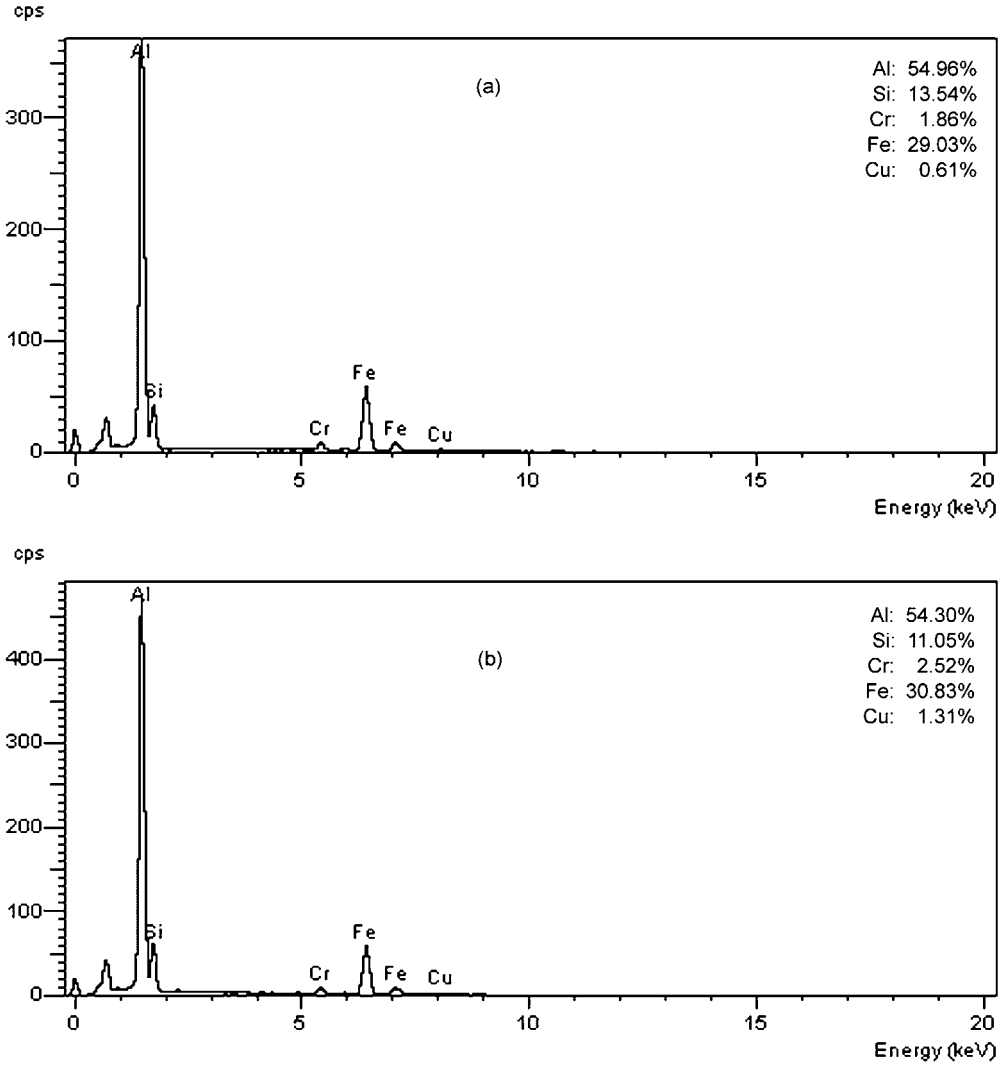

Figure 4 EDS spectra of the compact layer in (a) 0.15% Fe and (b) 0.60% Fe aluminium alloy.

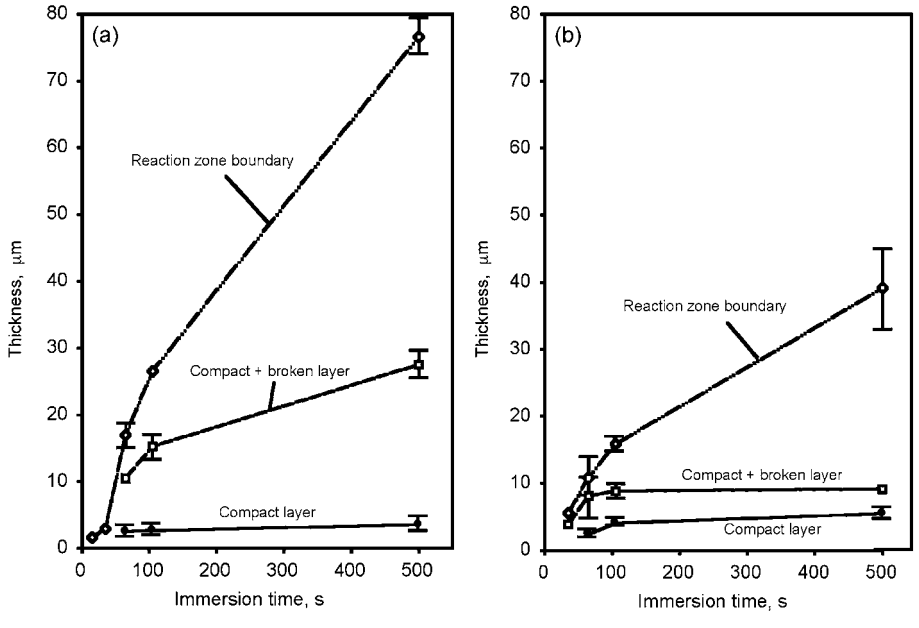

Figure 5 Thickness versus immersion time for H13 tool steel coupons immersed in an aluminium alloy melt containing (a) 0.15% Fe and (b) 0.60% Fe—the value for the reaction zone boundary represents its distance from the H13 interface. Error bars represent standard deviations.

layer (both semi-solid), and the reaction zone boundary (RZB). The original solid/liquid (OS/L) interface is designated as the origin, implying that $X_{\mathrm{OS/L}} \equiv 0$. The corresponding distances between the individual interface and the original solid/liquid interface, $X_{\mathrm{H13/CL}}$ (= IMD), $X_{\mathrm{CL/BL}}$ (CL = compact layer, BL = broken layer) and X_{RZB} for $t > 0$ are also shown in Fig. 7.

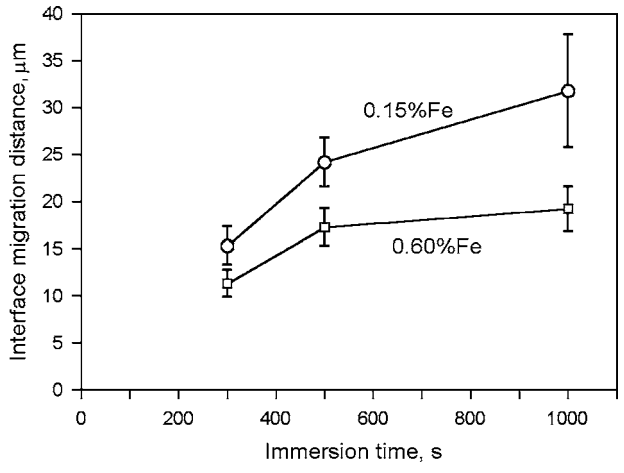

Figure 6 Interface migration distance versus immersion time for H13 tool steel immersed in both 0.15% Fe and 0.60% Fe aluminium alloy melts. Error bars represent standard deviations.

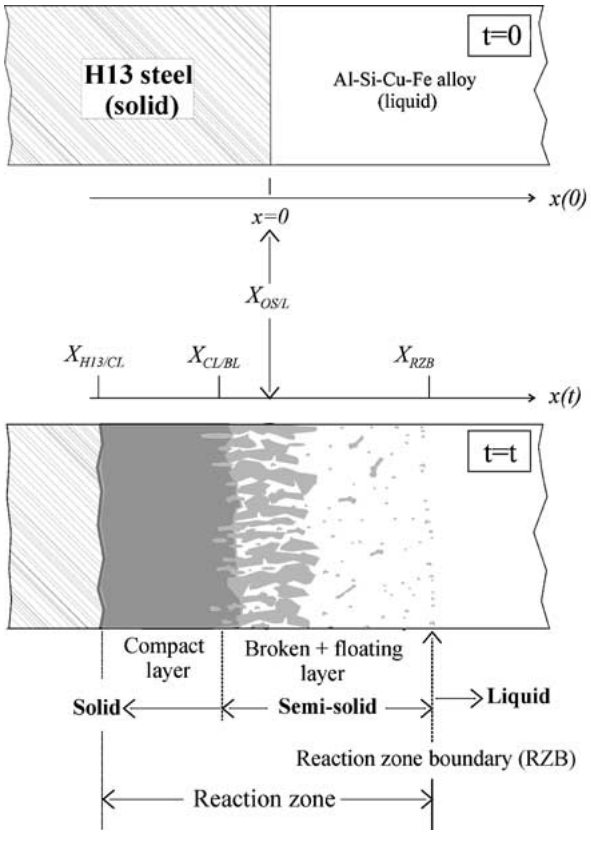

Figure 7 Schematic of the steel/aluminium alloy interface at time = t.

4.1. Effect of morphology on reaction rate

It is very clear from the results of the IMD-vs.-immersion time plots in Fig. 6 that the severity of reaction is significantly lower for the case of the higher iron melt. Additionally, this lower reaction rate was accompanied by a significantly thicker compact layer adjacent to the steel substrate (Figs 2, 3 and 5). The observation of an association between the intermetallic later growth morphology and the rate of the reaction is reasonable since the growth (migration of the steel/intermetallic interface) relies on the diffusion of atoms through the compact layer itself. As the diffusion coefficient for liquid metal can be up to 3–4 orders of magnitute higher than that in solid, the rate determining factor for the reaction is the rate of solid-state diffusion through the compact layer.

There appears to be no data available that describes the case of iron and aluminium diffusion in Fe-Al-Si ternery compounds [13]. For an Fe-Al alloy reaction couple, it is well known that Fe_2Al_5 is the dominant layer [13, 22]. The rate of diffusion for aluminium in Fe_2Al_5, according to Lamkov [23] and Lamkov *et al.* [24], is likely to be much greater than iron. We may also assume that the rate of diffusion of aluminium in Fe-Al-Si intermetallic compounds is much greater than iron and therefore examine the effect of aluminium diffusion on the present reaction rate.

We can examine the ideally steady state growth as illustrated in Fig. 8 and assume that $C_{\text{Al-1}}$ and $C_{\text{Al-2}}$, the concentrations in the compact layer at $X_{\text{H13/CL}}$ and $X_{\text{CL/BL}}$ (Fig. 7) respectively, are the same for both melts. Hence, the change in concentration of aluminium (Δc) will be the same in both melts and can be expressed as follows:

$$\Delta C = C_{\text{Al-2}} - C_{\text{Al-1}} \tag{1}$$

However, the thickness of the compact layer (Δx) differs for the two cases (i.e., $\Delta x_{0.15\%\text{Fe}} < \Delta x_{0.60\%\text{Fe}}$). It is reasonable to assume that D (the diffusion coefficient) in the compact layer is the same for both the low and the higher iron cases. Therefore:

$$\frac{\Delta c}{\Delta x_{0.15\%\text{Fe}}} > \frac{\Delta c}{\Delta x_{0.60\%\text{Fe}}} \tag{2}$$

According to Fick's 1st Law:

$$J = -D\left(\frac{\Delta c}{\Delta x}\right) \tag{3}$$

Thus, the flux of aluminium atoms passing through the compact layer will be greater in the lower iron case ($J_{0.15\%\text{Fe}} > J_{0.60\%\text{Fe}}$). This implies that the reaction rate measured by the IMD should be higher for the case of 0.15% Fe, as has been observed in Fig. 6.

Various authors (including [6–8]) have chosen to directly link the reaction extent or severity of the reaction with the thickness of the intermetallic layer. Reference to Fig. 3 shows that, for the case of H13 immersed for 500 s in both low and high iron alloy, the thickness of the (compact + broken) intermetallic layer is far greater in the low iron case (~25 μm) than in the high iron case (~9 μm). The logical assumption extending from this type of measurement is that the reaction severity is nearly three times as great in the lower iron case. However, our IMD data, a direct measure of steel removal, suggests that the reaction is only ~1.4 times the severity in low iron melts (~24 μm IMD as opposed to ~17 μm). The fraction solid during immersion partly explains this, since in the low iron case the broken layer is characterised by loose intermetallic containing a proportion of liquid aluminium alloy. Obviously, a lower fraction solid in the intermetallic layer implies that for a given amount of intermetallic product, the layer will appear "thicker". Hence, two

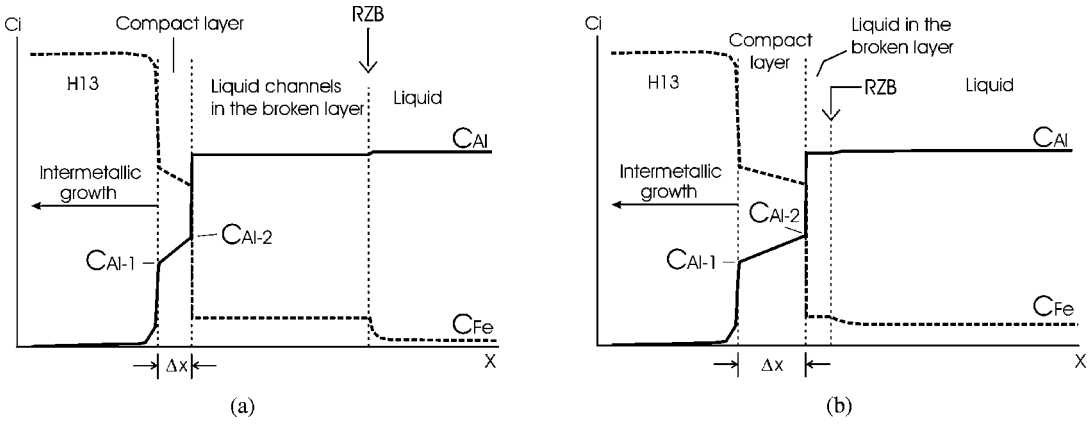

Figure 8 Schematic illustrations of the composition of aluminium and iron across the reaction layer from the H13 substrate to the melt during immersion in (a) 0.15% Fe alloy and (b) 0.60% Fe alloy melts.

inadequacies of using intermetallic thickness as a measure of reaction are:

- Dissolution of the layer, leading to underestimations of the reaction severity, and
- Differences in fraction-solid of intermetallics in the layer, leading to an overestimation of reaction extent.

An alternative method for assessing die steel consumption during immersion is the weight loss measurement, as used by Sundqvist *et al*. [9]. This method is based on the removal of the attached aluminium alloy and the intermetallic layers by chemical means and the measured weight difference of the coupon before and after immersion is the measure of the amount reacted. The results of this investigation are in disagreement with that of Sundqvist *et al*. [9], whose data showed that a lower iron content resulted in a lower reaction rate by way of weight measurement. There was, however, no evidence by Sundqvist *et al*. [9] confirming whether or not the iron-rich intermetallic layer was actually removed completely, without etching away any of the steel substrate. The direct measurement of IMD as a function of immersion time, as performed in this study, is seen as a more accurate and direct method of determining the extent of reaction.

4.2. Effect of concentration difference on reaction

As discussed above, the results of the present study have shown that a higher iron content has resulted in a thicker compact layer, which has acted as a diffusion barrier and hence reduced the rate of reaction. We now attempt to understand the mechanism for the differences in the intermetallic morphology in the whole reaction zone (RZ). We first examine the interface between the compact layer and the broken layer, $X_{\mathrm{CL/BL}}$ in Fig. 7. The results of a previous study in an iron saturated melt [3] may provide a useful insight into the observations of the current investigation, despite the longer immersion times (5 h) and higher melt temperature used. The intermetallic morphology in that study [3] consisted of an inner compact layer, an outer compact layer, and a thick composite layer. The latter is similar to the combination of the broken and floating layer in the present work.

Using X-ray diffraction, the outer compact layer was identified as a phase isomorphous with the commonly known α_{H} (Al-Fe-Si) ternary phase with a hexagonal structure [3]. The intermetallic in the composite layer was identified as α-phase, yet exhibited a body-centred cubic structure (α_{bcc}). Chen *et al*. [3] present analytical data to show that the thin α_{H} phase compact layer contained lower chromium and copper content ($\approx$1.5 and $\approx$0.3% respectively) than the α_{bcc} phase contained within the composite layer ($\approx$3 and $\approx$1.7% respectively). Manganese content was also lower in the α_{H} phase than in the α_{bcc} phase. These compositional changes are consistent with the established phenomenon [25, 26] that chromium, manganese and copper stabilize a cubic structure (α_{bcc} phase) at the expense of the hexagonal structure (α_{H} phase).

The transformation occurs at the boundary of the outer compact phase and the composite layer [3]. Thus, it takes place in the presence of liquid aluminium alloy in the composite layer. The suggestion may be made that equilibrium exists between α_{H} phase, α_{bcc} phase and liquid aluminium alloy. Observation of the interface in the current work suggests that the same destabilizing mechanism as observed by Chen *et al*. [3] may be occurring, particularly for samples with the longer immersion times. Thus, it may be suggested that the following transformation takes place:

$$\alpha_{\mathrm{H}} \rightarrow \alpha_{\mathrm{bcc}} + \mathrm{L}. \tag{4}$$

This reaction should result in the $\alpha_{\mathrm{H}}/(\alpha_{\mathrm{bcc}} + \mathrm{L})$ interface moving towards the substrate. As shown in Fig. 5 and referring to Fig. 7, the compact layer thickness ($|X_{\mathrm{H13/CL}} - X_{\mathrm{CL/BL}}|$) following 500 s immersion is only 2–3 μm and $\sim$6 μm for the low and high iron contents respectively. As shown in Fig. 6 and also referring to Fig. 7, for the same immersion time, $|X_{\mathrm{H13/CL}}|$ (= IMD) was $\sim$17 and $\sim$24 μm, for high and low iron cases respectively. Hence, $X_{\mathrm{CL/BL}}$ must have moved significantly towards the H13 substrate, consistent with the suggestion of the broken layer/compact layer interface is also the $\alpha_{\mathrm{H}}/(\alpha_{\mathrm{bcc}} + \mathrm{L})$ interface.

We now examine the other side of the reaction zone, i.e. near the RZB (see Figs 7 and 8). During immersion,

the liquid inside the RZB is clearly saturated with a combination of iron and chromium (as evidenced by the floating intermetallic particles). The solubility of the combined Fe + Mn+ Cr should follow [27, 28]:

$$S_{\mathrm{Fe+Mn+Cr}} = (\%\mathrm{Fe}) + 2(\%\mathrm{Mn}) + 3(\%\mathrm{Cr}) \quad (5)$$

where $S_{\mathrm{Fe+Mn+Cr}}$ is the solubility of Fe + Mn + Cr above which an (Al-Si-Fe-Mn-Cr) intermetallic compound forms. In our case, we can modify the equation to:

$$S_{\mathrm{Fe+Cr}} = (\%\mathrm{Fe}) + 3(\%\mathrm{Cr}) \quad (5a)$$

since %Mn ≈ 0 in the original melt and very low in H13. Analysing data from Granger [24] shows that, at 610°C, $S_{\mathrm{Fe+Cr}} \approx 1.4$. However, the upper bound value of %Cr above which Equation 5 no longer applies is not clear.

We first examine a simplified situation where the RZB is close to being stationary and close to the original solid/liquid interface, and consider only the diffusion of iron. Further, we consider the saturation concentration of iron to be 1.2% (taking a small amount of Cr into account), a level that is maintained inside the RZB. Hence, across the RZB, we have:

$$\Delta c_{\mathrm{s\text{-}o}} = 1.2 - c_{\mathrm{o}} \quad (6)$$

where c_{o} is the initial iron concentration in the bulk of the melt outside the RZB. The concentration of iron on the unsaturated side (i.e., outside the RZB) is $c_{\mathrm{Fe}}(x, t)$, where x is the distance from the RZB and t is time. Solving Fick's second law with the boundary condition given and integrating $c_{\mathrm{Fe}}(x, t)$ from 0 to ∞ with respect to x yields:

$$Q_{\mathrm{Fe}} = \frac{2}{\pi} \cdot \Delta c_{\mathrm{s\text{-}o}} \cdot \sqrt{D_{\mathrm{L}} \cdot t} \quad (7)$$

where Q_{Fe} is the amount of iron per unit area having diffused through the RZB at time t, and D_{L} is the diffusion coefficient of iron in the liquid. Then:

$$\frac{Q_{\mathrm{Fe}}(0.15\%\mathrm{Fe})}{Q_{\mathrm{Fe}}(0.60\%\mathrm{Fe})} \approx 1.75$$

This figure compares closely with the ratio of means for the interface migration distances:

$$\frac{\mathrm{IMD}_{0.15\%\mathrm{Fe}}}{\mathrm{IMD}_{0.60\%\mathrm{Fe}}} \approx 1.7$$

for immersion time at 1000 s, although the RZB is clearly not stationary and iron stored in the RZ is different for the two melts. The close comparison between the calculated flux ratio and the IMD ratio may simply suggest that the greater concentration difference in the lower iron melt results in a greater driving force for diffusion, and hence is one of the major factors for a higher reaction rate.

We now consider that the RZB is not stationary but has actually moved to the melt side from the original solid/liquid interface. Referring to Figs 5 and 6 for the individual measurement (*h*), for 500 s immersion:

$$\text{for } 0.15\%\mathrm{Fe} \quad X_{\mathrm{RZB}} = h_{\mathrm{RZB}} - h_{\mathrm{IMD}} \approx 77 - 24 = 53\ \mu\mathrm{m}$$

and

$$\text{for } 0.60\%\mathrm{Fe} \quad X_{\mathrm{RZB}} = h_{\mathrm{RZB}} - h_{\mathrm{IMD}} \approx 39 - 19 = 20\ \mu\mathrm{m}$$

This implies that the amount of Fe + Cr released to the melt in the RZ from the intermetallic growth is larger than the amount transferred from the RZ to the bulk of the melt. Hence, for mass balance, $X_{\mathrm{RZB}} > 0$.

We now consider Equation 4 ($\alpha_{\mathrm{H}} \rightarrow \alpha_{\mathrm{bcc}} + \mathrm{L}$, the compact to broken layer morphological transformation). Solubility of chromium in α_{H} is likely to be approximately 1.5% [3], but there is 5% Cr in the H13 substrate. Hence, the growth of the compact layer towards the substrate should result in the supersaturation of chromium in α_{H} compact layer, favouring transformation (Equation 4), as α_{bcc} allows a significantly higher chromium content (~3%). The liquid associated with the transformation should also be saturated with chromium. On the other hand, the transformation must result in the release of iron into the liquid, as the iron content in α_{bcc} is ~8% lower than that in α_{H} [3]. The higher outward diffusion of iron to the bulk alloy in the lower iron case (as suggested above) can then assist the transformation. This transformation in turn results in thinning of the compact layer. Hence, it is reasonable for a thinner and a more uneven compact layer (due to local transformation) to be observed for the low iron case.

Referring again to the RZB, the reason for $X_{\mathrm{RZB}} > 0$ and $X_{\mathrm{RZB\text{-}0.15Fe}} > X_{\mathrm{RZB\text{-}0.60Fe}}$ is not clear. As stated before, possible maximum solubility of chromium is not known. In the absence of further data on chromium content in the melt within the RZ, accurate consideration concerning diffusion can not be made. Data by Granger [16] shows that for an alloy (%Si close to ours) containing 0.63% Fe, 0.3%Mn and 0.08%Cr the equilibrium %Cr is approximately 0.05 at 610°C. (Our unpublished data in a previous study suggests that the chromium content for an alloy containing 1.2% Fe, 0.21%Mn, 0.035%Cr is less than 0.02% at 610°C). It is possible that the upper limit of chromium content is a very low value for the application of Equation 5.

For the diffusion of chromium, Equation 6 shall also apply, if we take instead Q_{Cr} and a chromium-specific D_{L}. A low value of %Cr within the RZ means a low value of $\Delta c_{\mathrm{s\text{-}o}}$ and hence low value of outward diffusion. As described above, $\alpha_{\mathrm{H}} \rightarrow \alpha_{\mathrm{bcc}}$+ L transformation will always enrich the liquid with chromium. If the rate of chromium diffusion to the bulk melt is less than that released due to the transformation at $X_{\mathrm{CL/BL}}$, a wider RZ where (%Fe) + 3(%Cr) = 1.4 could result. This may be the reason for the widening RZ and hence $X_{\mathrm{RZB}} > 0$, as well as $X_{\mathrm{RZB\text{-}0.15Fe}} > X_{\mathrm{RZB\text{-}0.60Fe}}$, as transformation at $X_{\mathrm{CL/BL}}$ is assisted by a higher rate of outward diffusion of iron for the low iron case.

5. Conclusions

The major differences between the interfacial intermetallic morphologies observed for the reaction between H13 tool steel and an Al-11Si-2.5Cu melt containing 0.15 and containing 0.60% Fe at 610°C is the relative thickness of the compact and broken layers. The compact layer is thicker and the broken layer is considerably thinner for the higher iron case. The thicker compact layer for the higher iron melt is consistent with the observed lower intermetallic/substrate migration distance, meaning less consumption of the substrate. We explain this in terms of a thicker compact (solid) intermetallic layer providing a larger reduction in the diffusion flux and hence lower reaction rate. We propose that the larger broken layer and a small compact layer for the case of low iron are due to a higher diffusion rate of iron from the compact/broken layer interface to the liquid in the wider reaction zone, balanced by the rate of transformation at the compact/broken layer interface. It is proposed that the low rate of diffusion of chromium may have resulted in a widening reaction zone.

Acknowledgments

This work was funded by the Cooperative Research Centre for Cast Metals Manufacturing (CAST), which was established under and is supported by the Australian Government's Cooperative Research Centers Program.

References

1. K. VENKATESAN and R. SHIVPURI, in Transactions of the 18th International Casting Congress and Exposition, Indianapolis, 1995 (NADCA, Rosemont, 1995) Paper 106.
2. J. A. TAYLOR, D. H. StJOHN, J. BARRESI and M. J. COUPER, *Intern. J. Cast Met. Res.* **12** (2000) 409.
3. Z. W. CHEN, D. T. FRASER and M. Z. JAHEDI, *Mater. Sci. Engin.* A **260** (1999) 188.
4. Y. CHU, P. S. CHENG and R. SHIVPURI, in Transactions of the 17th International Casting Congress and Exposition, Cleveland, 1993 (NADCA, Rosemont, 1993) Paper 124.
5. L. NORSTROM, B. KLARENFJORD and M. SVENSSON, in Transactions of the 17th International Casting Congress and Exposition, Cleveland, 1993 (NADCA, Rosemont, 1993) Paper 75.
6. S. SHANKAR and D. APELIAN, in Transactions of the 17th International Casting Congress and Exposition, Cleveland, 1993 (NADCA, Rosemont, 1993) Paper 85.
7. *Idem.*, in Proceedings of the 5th International Molten Metal Conference, Orlando, 1998 (AFS 1998) p. 281
8. *Idem.*, in Transactions of the 20th International Casting Congress and Exposition, Cleveland, 1999 (NADCA, Rosemont, 1999) paper 83.
9. M. SUNDQVIST, J. BERGSTROM, T. BJORK and R. WESTERGARD, in Transactions of the 19th International Casting Congress and Exposition, Minneapolis, 1997 (NADCA, Rosemont, 1997) Paper 104.
10. M. SUNDQVIST and S. HOGMARK, *Trib. Intern.* **26** (1993) 129.
11. M. YU, Y. CHU and R. SHIVPURI, in Transactions of the 17th International Casting Congress and Exposition, Cleveland, 1993 (NADCA, Rosemont, 1993) Paper 72.
12. M. YAN and Z. FAN, *J. Mater. Sci.* **35** (2000) 1661.
13. *Idem.*, *ibid.* **36** (2001) 285.
14. Z. W. CHEN and M. Z. JAHEDI, *Intern. J. Cast Met. Res.* **11** (1998) 129.
15. J. A. TAYLOR, G. B. SCHAFFER and D. H. StJOHN, *Metall. Mater. Trans.* A **30A** (1998) 1651.
16. G. A. GRANGER, in Transactions of the 95th American Foundry Society Casting Congress, Birminghan, 1991 (AFS, Des Plaines, 1991) p. 379.
17. S. G. DENNER and R. D. JONES, *Met. Techn.* **4** (1977) 167.
18. G. EGGELER, W. AUER and H. KAESCHE, *J. Mater. Sci.* **21** (1986) 3348.
19. *Idem.*, *Z. Metallkde* **77** (1986) 239.
20. N. A. EL-MAHALLAWAY, M. A. TAHA, M. A. SHADY, A. R. EL-SISSI, A. N. ATTIA and W. REIF, *Mater. Sci. Techn.* **13** (1997) 832.
21. G. B. WINKELMAN, Z. W. CHEN, D. H. StJOHN and M. Z. JAHEDI, to be submitted to *J. Mater. Sci. Lett.*
22. R. W. RICHARDS, R. D. JONES, P. D. CLEMENTS and H. CLARKE, *Intern. Mater. Rev.* **39** (1994) 191.
23. L. N. LAMKOV, *Avtom. Svarka* **24** (1971) 64.
24. L. N. LAMKOV, V. M. FALCHENKO, D. F. POLISHCHUK, V. R. RYABOV and A. V. LOZOVSKYA, *ibid.* **3** (1970) 66.
25. L. F. MONDOLFO, "Aluminium Alloys: Structure and Properties" (Butterworths, London, 1976).
26. V. G. RIVLIN and G. V. RAYNOR, *Intern. Met. Rev.* **3** (1981) 133.
27. S. G. SHABESTARI and J. E. GRUZLESKI, in Proceedings of the International Symposium on Light Alloy Metals: Processing and Applications, Quebec, 1993 (CIM, Quebec, 1993) p. 241.

Received 30 December 2002
and accepted 18 August 2003